Entrance Channel Stereospecificity of Photoinitiated H-Atom Reactions in Weakly Bonded Complexes

Seung Koo Shin, Y. Chen, D. Oh and C. Wittig

| **Email alerting service** | Receive free email alerts when new articles cite this article - sign up in the box at the top right-hand corner of the article or click **here** |

Entrance channel stereospecificity of photoinitiated H-atom reactions in weakly bonded complexes

By Seung Koo Shin, Y. Chen, D. Oh and C. Wittig

Department of Chemistry, University of Southern California, Los Angeles, California 90089-0482, U.S.A.

Hot H-atom reactions photoinitiated in T-shaped CO_2–HBr and nearly-linear CO_2–HCl complexes show remarkably different reaction probabilities. Broadside H-atom approaches in CO_2–HBr complexes are greatly favoured over the relatively end-on approaches of CO_2–HCl complexes, a striking steric effect. Photoinitiated hot H-atom reactions with N_2O result in a much lower [NH]/[OH] ratio with N_2O–HI complexes than under single-collision conditions at the same photolysis wavelength. In addition, OH rotational distributions differ markedly between bulk and complexed conditions, while NH rotational distributions are similar. These results can be interpreted in terms of entrance channel stereospecificity influencing chemically distinct product channels.

1. Introduction

It has been widely appreciated that elementary chemical reaction dynamics in the gas phase depend strongly upon the relative orientations, alignments and velocities of the approaching reactants (Levine & Bernstein 1987). These entrance-channel parameters can determine the reaction pathways on the potential energy surface (PES) and influence overall cross-sections, branching ratios, and product state distributions (PSDs). However, in most gaseous collision environments, there is no control over incident angles and impact parameters. Pioneering attempts to control entrance-channel geometric properties utilizing the interaction of the molecule with external electric or magnetic fields have yielded exciting results for specific alignments and orientations. (Kramer & Bernstein 1965; Beuhler et al. 1966; Brooks 1969, 1976; Marcelin & Brooks 1975; Karny et al. 1976; van den Ende & Stolte 1980; Parker et al. 1981, 1987; Stolte 1982, 1987; Zare 1982; Rettner & Zare 1982; Gandhi et al. 1986, 1987; Johnson et al. 1986).

Our research in this area has exploited the intermolecular interaction present in weakly-bonded reaction-precursor complexes. (Jouvet & Soep 1983; Breckenridge et al. 1986; Duval et al. 1986; Zehnacker et al. 1987; Jouvet et al. 1987; Buelow et al. 1986, 1987; Radhakrishnan et al. 1986; Wittig et al. 1988; Chen et al. 1989, 1990a, b; Häusler et al. 1987; Hoffmann et al. 1989a, b). Since the anisotropic intermolecular force field binding the complex results in a stereospecifically aligned precursor geometry, such precursor-geometry-limited (PGL) reactions offer a novel means of investigating entrance channel effects (Wittig et al. 1988). In addition, photo-initiation provides control of the reaction energy by varying the photolysis wavelength, as well as setting the 'zero-of-time' of the reaction by using an

[173]
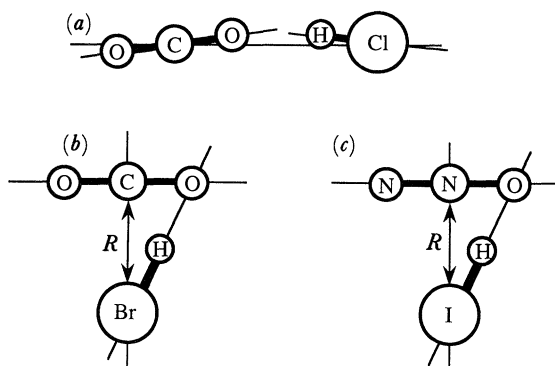
Figure 1. Schematic drawing depicting (*a*) end-on H-atom attack for CO_2–HCl, (*b*) broadside H-atom attack for CO_2–HBr and (*c*) broadside H-atom attack for N_2O–HI.

ultrashort laser pulse. (Zewail 1988; Zewail & Bernstein 1988). Recent advances in real-time clocking of bimolecular reactions have been accomplished by taking advantage of this new way of controlling reactions (Scherer *et al.* 1987, 1990).

In this discussion, we report studies of photoinitiated reactions of H atoms with CO_2 and N_2O using CO_2–HBr, CO_2–HCl and N_2O–HI complexes as precursors, as well as the corresponding bulk reactions. PSDs are interpreted in terms of the geometries of the weakly-bonded precursors, reaction intermediate lifetimes, exothermicities, reverse barrier heights that imprint dynamical bias on PSDs, and possible contributions from termolecular interactions. Variation of overall reaction probability with initial H-atom approach is examined using CO_2–HX complexes, and for the N_2O/HI system, changes in the [NH]/[OH] branching ratio between bulk and complexed conditions are reported that elucidate the entrance channel stereospecificity of photoinitiated reactions under complexed conditions.

Reactions of H atoms with CO_2 are endothermic by 25 kcal† mol^{-1} and have been extensively studied previously under both bulk and complexed conditions (Buelow *et al.* 1985, 1987; Radhakrishnan *et al.* 1986; Wittig *et al.* 1988; Chen *et al.* 1989; Flynn & Weston 1986; Quick & Tiee 1983; Kleinermanns & Wolfrum 1983*a*, *b*; Kleinermanns *et al.* 1985; Schatz *et al.* 1988; Schatz & Fitzcharles 1988):

$$H + CO_2 \rightarrow OH + CO \quad \Delta H_{298} = 8960 \text{ cm}^{-1}. \tag{1}$$
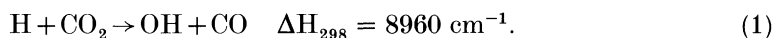
The choice of CO_2–HBr and CO_2–HCl complexes as precursors is due to their well-defined geometric differences, as shown in figure 1*a*, *b*. High-resolution infrared spectroscopic studies of these weakly-bonded complexes in our laboratory reveal that CO_2–HBr is asymmetric, with the Br–C line essentially perpendicular to the CO_2 axis and the H atom probably localized near one of the oxygens, while CO_2–HCl is near-linear with the hydrogen bonded to the oxygen (Sharpe *et al.* 1990). These two geometrically distinct precursors can provide fundamental understanding about different reaction probabilities for end-on H-atom approaches (CO_2–HCl) and broadside approaches (CO_2–HBr). Figure 2 shows the lowest barrier pathway diagram (Chen *et al.* 1989). The OH channel is characterized by an entrance barrier of 26 kcal mol^{-1}, a HOCO† intermediate (*ca.* 8 kcal mol^{-1} below $H + CO_2$), and a low reverse barrier (*ca.* 1 kcal mol^{-1}).
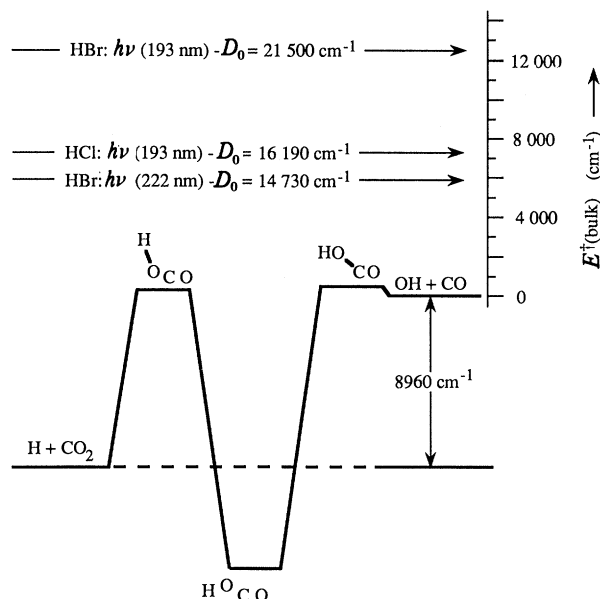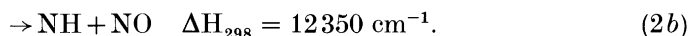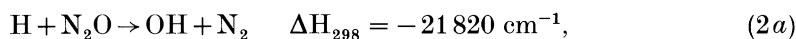
† 1 cal = 4.184 J.

Figure 2. Energy diagram showing relevant stationary points for the $\bar{H} + CO_2$ system (Chen *et al.* 1989*a*). $E^\dagger$ corresponds to the available energy in the product channel.

In reactions of hot H atoms with N_2O, (Hoffmann *et al.* 1989*a, b*; Chen *et al.* 1990*a, b*; Dixon-Lewis & Williams 1977; Hollingsworth *et al.* 1985; Marshall *et al.* 1987, 1989; Ohoyama *et al.* 1989) there are two chemically distinct pathways, the exothermic OH and endothermic NH channels:

$$H + N_2O \rightarrow OH + N_2 \quad \Delta H_{298} = -21\,820 \text{ cm}^{-1}, \tag{2a}$$

$$\rightarrow NH + NO \quad \Delta H_{298} = 12\,350 \text{ cm}^{-1}. \tag{2b}$$

The N_2O–HI structure is presumed similar to that of N_2O–HBr, for which R_{cm}, the separation between the N_2O and HBr centres-of-mass, is 3.64 Å†, and the angle between R_{cm} and the N_2O axis is 75–82° (Zeng *et al.* 1990). The broadside H-atom approach in this presumably 'T-shaped' precursor shown in figure 1*c* faces two different reaction pathways; either oxygen-side or nitrogen-side attack (Marshall *et al.* 1987, 1989). We emphasize that the N_2O–HI structure has not been measured, and even with N_2O–HBr, the H atom could not be located experimentally. Thus the structure shown in figure 1*c* should be considered an, as yet, unproven possibility. It is very unlikely that a linear counterpart of FH–NNO exists for HBr or HI complexes, but there are certain other possibilities besides the one shown in figure 1*c*.

Attack on the oxygen side encounters an entrance barrier of at least 20 kcal mol^{-1} and abstracts oxygen directly without formation of a long-lived intermediate, as shown in figure 3. The reaction exothermicity, combined with the entrance barrier, leads to the high reverse barrier for the OH product channel. Nitrogen-side approach can confront a lower entrance barrier than the oxygen-side attack, forming a HNNO† intermediate (i.e. HNNO is 15 kcal mol^{-1} below $H + N_2O$). This intermediate can undergo 1,3-hydrogen-migratory decomposition to yield $OH + N_2$ or decompose

† 1 Å = 10^{-10} m = 10^{-1} nm.

Figure 3. Energy diagram showing relevant stationary points for the $H + N_2O$ system (Marshall *et al.* 1987, 1989). The c.m. collision energies corresponding to different HI photolysis wavelengths are for $H + I(^2P_{\frac{3}{2}})$ channel only.

to $NH + NO$ by overcoming the high exit channel barrier. Therefore, photoinitiated H-atom reactions with N_2O afford the possibility of observing a change in the chemically distinct product branching ratio in going from the isotropic bulk to the stereospecific complexed PGL conditions.

2. Experimental

The experimental arrangement shown in figure 4 was described elsewhere in detail (Radhakrishnan *et al.* 1986). With both bulk and PGL conditions, photolysis was followed by LIF product detection. Photoinitiation was achieved using either excimer lasers (e.g. 193 and 222 nm) or a frequency doubled dye laser (BBO doubling crystal), tunable throughout the region 220–280 nm. Effectively monoenergetic H atoms (*vide infra*) are produced by HX (X = Cl, Br, and I) photolysis. The probe beam was from the doubled output of a Nd:YAG pumped dye laser.

Bulk reactions were studied in flowing samples, typically 30% HX and 70% CO_2 or N_2O at *ca.* 40 mTorr† total pressure. To ensure single-collision, arrested-relaxation conditions, short delays (*ca.* 100 ns) between the photolysis and probe lasers were used. Under these conditions, nascent H atoms undergo *ca.* 0.3 hard sphere collisions on average and nascent products are subject to *ca.* 0.03 collisions on average. As reported previously, our results are unaffected by either an increase or decrease of a factor of 2 in either delay or total pressure (Radhakrishnan *et al.* 1986). Weakly bonded complexes were prepared by expanding mixtures of typically 3% HX, 5% CO_2 or 7% N_2O, and the balance He through a pulsed nozzle (2 atm‡ stagnation pressure) into a vacuum chamber. These complexes were monitored with a quadrupole mass spectrometer and expansion conditions were adjusted so that the

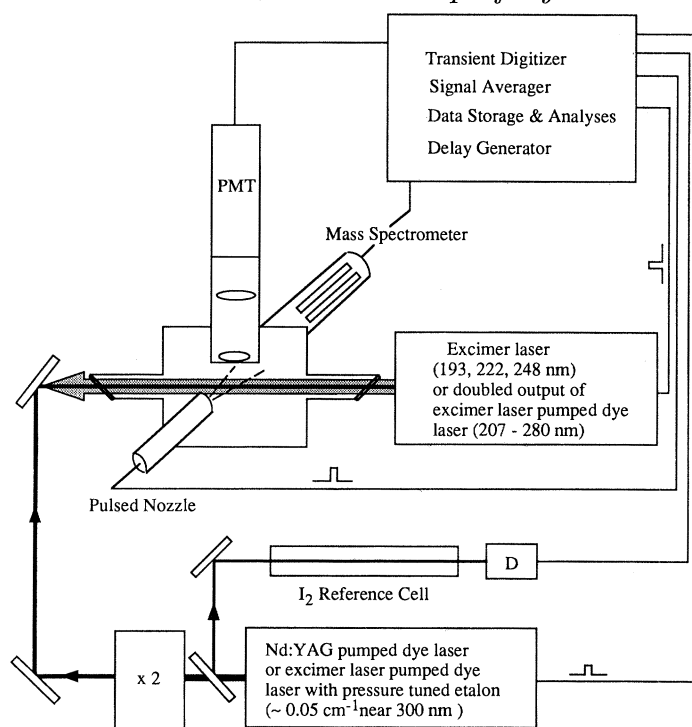† 1 Torr $\approx$ 133.3 Pa.   ‡ 1 atm $\approx$ 10⁵ Pa.

Figure 4. Schematic drawing of the experimental arrangement.

binary complex ions were more abundant by approximately an order of magnitude than the tertiary mixed complex ions. Typical photolysis-probe delays of *ca.* 60 ns were used for complexed conditions. In separate experiments, the mass-spectral intensities of CO_2-HX^+ ions were compared with their infrared (IR) absorption intensities using high-resolution infrared tunable diode laser spectroscopy to estimate the relative concentrations of the CO_2-HBr and CO_2-HCl clusters quantitatively. Note that Ar was used as a carrier gas with a pulsed slit nozzle in this experiment.

It has never been possible to completely eliminate contributions from higher-than-binary complexes in these experiments. Their presence is made clear by mass spectrometer signals corresponding to the higher (usually tertiary) complexes. With CO_2-HCl, they play no role, since we see essentially no signal. With CO_2-HBr, however, there may well be contributions that are manifest in the OH PSDs and overall reaction yields. However, we do not believe that they would alter any of our conclusions for the CO_2-HX or N_2O-HI systems reported here.

3. Results and Discussion

$H + CO_2$: *relative reaction probabilities for end-on and broadside approaches*

Photoinitiated reactions of H atoms with CO_2 were studied using CO_2-HCl complexes at 193 nm and CO_2-HBr complexes at both 193 and 222 nm. In addition, bulk reactions were compared with their PGL counterparts to evaluate the reaction probabilities for end-on and broadside approaches of hydrogen under PGL conditions. Since $h\nu - D_0(HX)$ is rather similar for 193 nm HCl and 222 nm HBr photolyses ($16\,100$ and $14\,800$ cm^{-1} respectively), these two cases can be meaningfully compared.
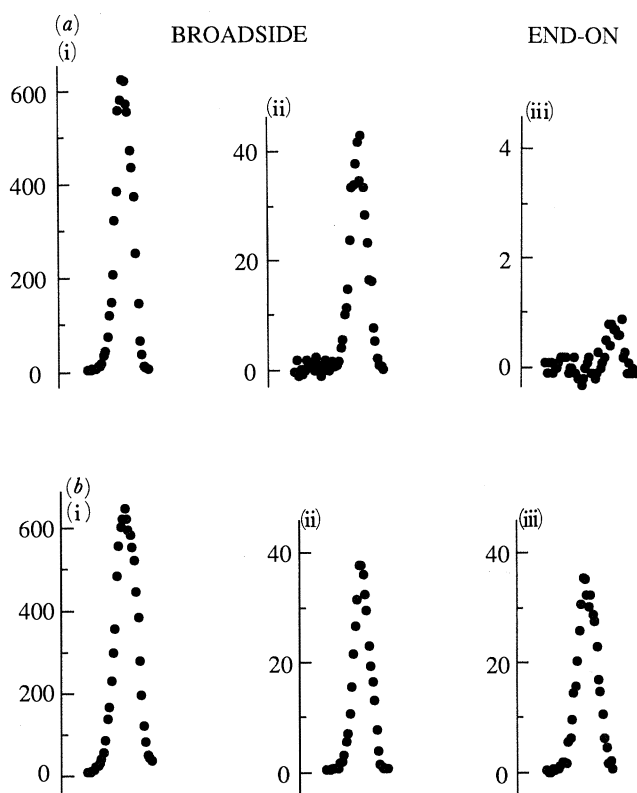
Figure 5. OH $A^2\Sigma \leftarrow X^2\Pi$ (0,0) LIF spectra (Q branch bandhead: $Q_{11}(7) + Q_{22}(2) + Q_{22}(3)$) of CO_2/HX system (*a*) under PGL conditions (typically averaging 20 shots per point for CO_2–HBr, and 200 shots per point for CO_2–HCl) and (*b*) under bulk conditions (typically 20–40 shots averaged per data point). In (*a*) $h\nu - D_0$(HBr) = 21 500 cm^{-1} (i), 14 730 cm^{-1} (ii) and 16 190 cm^{-1} (iii). In (*b*) E_{cm} = 20 760 cm^{-1} (i), 14 220 cm^{-1} (ii) and 15 390 cm^{-1} (iii).

Although steric effects have been known and acknowledged for a long time (Smith 1980), it has not been previously possible to experimentally arrange such different entrance channels as those shown in figure 1*a*, *b*.

OH $A^2\Sigma \leftarrow X^2\Pi$ (0,0) LIF spectra (Q branch bandhead: $Q_{11}(7) + Q_{22}(2) + Q_{22}(3)$) obtained with three different photoinitiated reactions under PGL conditions are presented in figure 5*a*. The experimental peak heights were converted to the total OH population using OH state distributions (D. Oh, H. Iams and C. Wittig, unpublished) and normalized using the relative HX absorption cross sections, laser fluences, relative CO_2–HCl and CO_2–HBr complex concentrations, etc. Results are summarized in table 1. Note that the [CO_2–HCl]/[CO_2–HBr] concentration ratio was evaluated by comparing the observed [CO_2–HCl$^+$]/[CO_2–HBr$^+$] mass spectral signal ratio with the integrated rovibrationally-resolved absorptions corresponding to the CO_2 asymmetric stretching mode of CO_2–HX complexes. After correcting for various experimental parameters, the estimated relative reaction probabilities are 370:100:2.4 for the respective PGL conditions of (CO_2–HBr)$_{193}$:(CO_2–HBr)$_{222}$: (CO_2–HCl)$_{193}$. Results from bulk reactions are shown in figure 5*b* for comparisons. The corrected reaction probabilities for various experimental parameters are 440:100:140
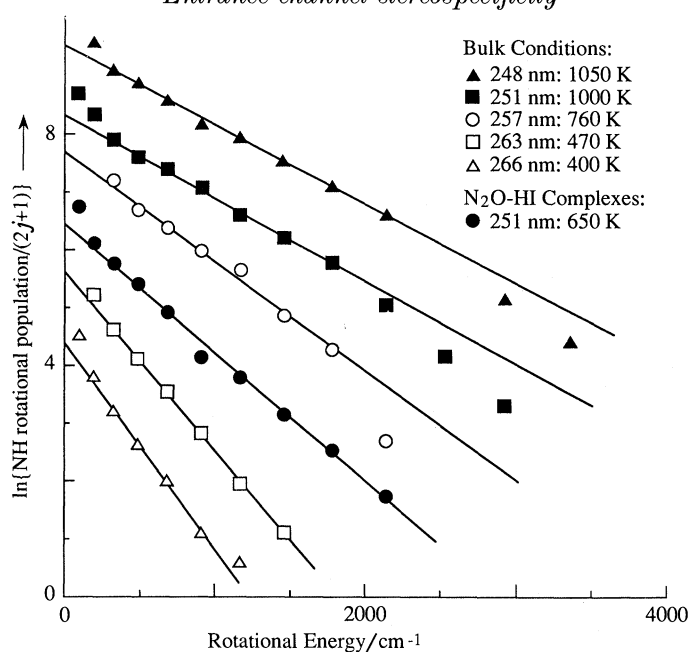
Figure 6. Logarithmic plots showing NH rotational distributions obtained at different photolysis wavelengths. Dark circles are for N_2O–HI complexes; the other data were obtained using bulk conditions.

Table 1. *Amounts of* OH *produced from photoinitiated reactions in* CO_2–HCl *and* CO_2–HBr *complexes*

	HBr (193 nm)	HBr (222 nm)	HCl (193 nm)
$\sigma_{absorption}/(10^{-19}\ cm^2)^a$	8.2	1.0	0.8
$h\nu - D_0(HX)/cm^{-1\ b}$	21 400	14 700	16 100
OH signal (arbitrary units)^c	850	57	1
fraction of OH in probed levels (%)	3.3	6.7	6.2
[OH] (arbitrary units)	1600	53	1
$[OH]/\sigma_{absorption}$ (arbitrary units)	370	100	2.4
$[CO_2$–HX] (arbitrary units)^d	1	1	$\approx 1^e$

^{a} 300 K samples. It is assumed that vibrational hot bands do not contribute.

^{b} For the $Br(^2P_{\frac{3}{2}})$ and $Cl(^2P_{\frac{3}{2}})$ (i.e. ground state) channels.

^{c} Recorded at the $Q_{11}(7) + Q_{22}(2) + Q_{22}(3)$ bandhead.

^{d} Based on CO_2HX^+ mass spectrometer signals, which are calibrated against high-resolution IR diode laser spectra of CO_2–HX complexes. The IR spectra give reliable CO_2–HCl and CO_2–HBr relative concentrations.

^{e} A lower bound of 0.3 is estimated for these measurements.

for the bulk counterparts of the three different PGL conditions respectively. It is quite striking to observe that the reaction probability with the CO_2–HCl system decreases by a factor of 60 in going from bulk to complexed conditions, while the relative reaction probability ratio for the two different CO_2–HBr complexed conditions is close to that for the corresponding bulk reactions, within experimental errors.

It is known that strictly linear $H + CO_2$ approaches are repulsive, whereas broadside approaches can access both HOCO and HCO_2 (C_{2v} equilibrium geometry), where the latter can convert to HOCO and then fragment to OH + CO (Schatz *et al.* 1987; Shatz & Fitzcharles 1988). So maybe it should come as no surprise that the

Phil. Trans. R. Soc. Lond. A (1990)

[179]
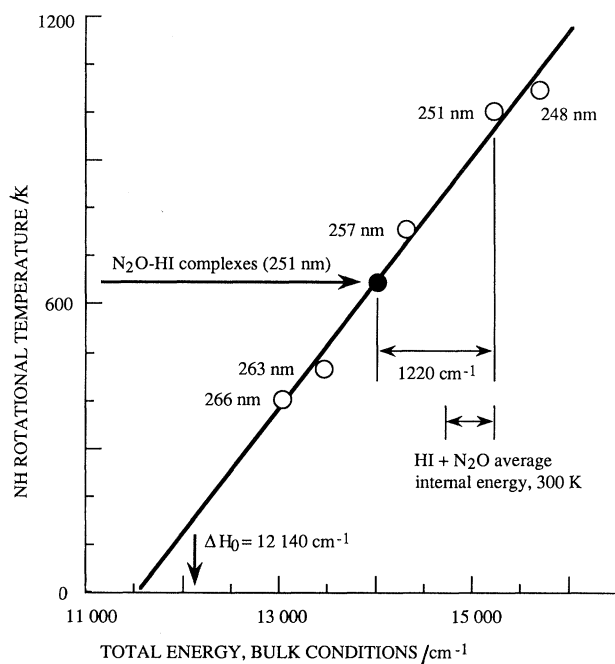
368 *Seung Koo Shin and others*

Figure 7. Plot of observed NH rotational temperature against E_{total} for bulk conditions. Note that 300 K bulk samples contain *ca.* 410 cm^{-1} of rotational energy, while complexes have essentially no internal energy except zero-point, and are also bound relative to free $N_2O + HI$. A straight line extrapolation comes close to the 0 K enthalpy change for this endoergic channel.

broadside configuration is favoured. This result may be ascribed to the stereo-electronic effect that a hydrogen atomic orbital makes good overlap with a CO π-orbital in overcoming a barrier, while it poorly overlaps with an oxygen σ-orbital lying in the CO_2 molecular axis. The term stereoelectronic refers to the effect of orbital overlap requirements on the steric course of a reaction (Lowry & Richardson 1981). An order of magnitude difference in reaction probability is a quite large steric effect at this energy, and should spur theorists to examine these results. Such entrance-channel specificity also has its counterpart in situations where different products from the same broadside approach might be formed, such as the $N_2O–HI$ systems presented below.

$H + N_2O$: *the orientation effect in broadside approach*

Reactions of H atoms with N_2O were studied with both bulk and complexed conditions using 251 nm photolysis of HI (Chen *et al.* 1990). The choice of 251 nm is a compromise between maximizing the H atom concentration and minimizing an OH $A^2\Sigma \rightarrow X^2\Pi$ chemiluminescence background that complicates LIF detection, even though OH($A^2\Sigma$) is a minor channel. 251 nm HI photodissociation yields $I(^2P_{\frac{3}{2}})$ (48%) and $I(^2P_{\frac{1}{2}})$ (53%) (van Veen *et al.* 1983) with corresponding H-atom kinetic energies of 15300 and 7700 cm^{-1}. NH $A^3\Pi \leftarrow X^3\Sigma$ (0,0) and OH $A^2\Sigma \leftarrow X^2\Pi$ (0,0) LIF spectra were converted to rotational level distributions using published line strengths (Chidsey & Crosley 1980; Dimpfl & Kinsey 1979; Dixon 1959; Fairchild *et al.* 1984) after correcting for photolysis and probe laser energies. The endoergic NH channel was further examined using tunable HI photolysis under bulk conditions.

Figure 6 shows several of the measured rotational distributions under bulk
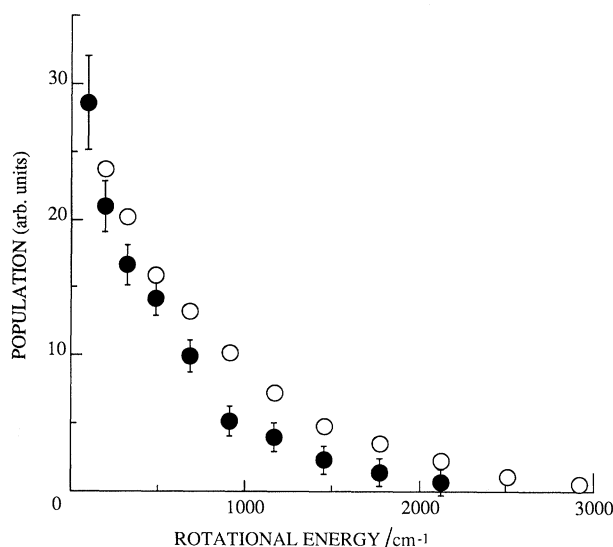
[180]

Figure 8. NH rotational distributions for bulk and complexed conditions using 251 nm HI photolysis. •, complexes; ○, bulk.

conditions obtained using tunable HI photolysis, indicating a smooth decrease in rotational excitation with increasing photolysis wavelength. As presented in figure 6, the rotational distributions can be assigned temperatures, and figure 7 shows the variation of these observed NH rotational temperatures with the total energy that would be available under bulk conditions. This energy is given by (3), which accounts for (i) H-atom motion in the HI c.m. system, (ii) H-atom motion in the $H + N_2O$ c.m. system, and (iii) HI and N_2O 300 K rotational energies (Chen *et al.* 1990).

$$E = [(127/128)(44/45)\{h\nu - D_0(HI) + RT\} + RT]. \tag{3}$$

These temperatures vary linearly with $h\nu - D_0(HI)$, extrapolating to zero at $11\,600$ cm^{-1}, close to ΔH_0 ($12\,100$ cm^{-1}) (Anderson 1989) for this endoergic channel. This statistical nature of NH rotational distributions indicates that the $NH + NO$ channel probably proceeds via a long-lived HNNO† intermediate.

With N_2O-HI complexes, the NH rotational distributions do not differ from their bulk counterparts obtained at the same photolysis wavelength (251 nm), although the rotational excitation is slightly lower as shown in figure 8. Again, the rotational distributions under complexed conditions can be ascribed a temperature as shown in figure 6. When placed on the plot of rotational temperature against the total energy for bulk conditions, it corresponds to an energy 1200 cm^{-1} less than the 251 nm bulk reaction as shown in figure 7. Note that 300 K bulk samples have 410 cm^{-1} excess energy in the form of HI and N_2O rotations, which is not present in complexes. In addition, the N_2O-HI complex is bound by weak van der Waals interaction, which must be overcome in the photoinitiated reaction. The remaining difference {i.e. $1200 - 410 - D_0(N_2O-HI)$ cm^{-1}} can be easily accounted for by the squeezed-atom effect (Wittig *et al.* 1988). The possible role of nearby I atom should not be discounted however, and awaits further scrutiny.

In marked distinction from the endoergic $NH + NO$ channel, the highly-exoergic $OH + N_2$ pathway has a large reverse barrier of *ca.* $28\,800$ cm^{-1} as shown in figure 3. Once past the entrance barrier, there is no long-lived intermediate, so product state
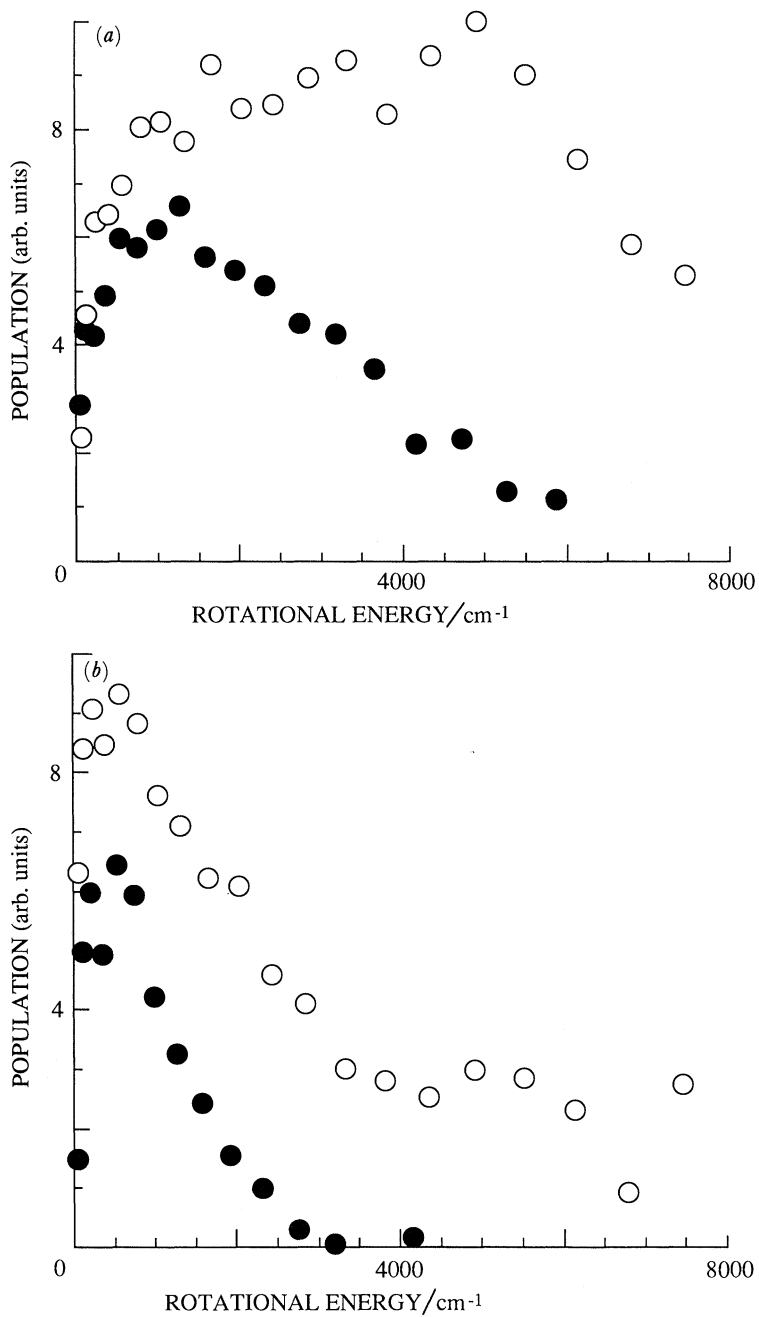
Figure 9. OH $v = 0$ and 1 rotational distributions obtained (*a*) under bulk conditions and (*b*) with N_2O–HI complexes (251 nm photolysis). Note the marked qualitative change, compared with the NH case shown in figure 8. $\circ$, $v = 0$; $\bullet$, $v = 1$.

distributions can be biased by the large reverse barrier. Therefore, there is no reason to expect statistical allocations of the total energy, and with so much energy, an extremely large number of product states might be occupied. The OH $v = 0$ and 1 rotational distributions for bulk conditions (251 nm photolysis) are shown in figure 9 for rotational levels up to the experimental limit imposed by OH $A^2\Sigma$ predissociation ($N \approx 20$ for $v = 0$ and $N \approx 19$ for $v = 1$) (Chidsey & Crosley 1980). Indeed, OH internal excitation is very high: the $[v = 1]/[v = 0]$ concentration ratio is *ca.* 0.5 for the observed rotational state, and $v = 0$ rotational excitation is very broad, extending almost certainly past the highest observed states. Vibrational levels above $v = 1$ must be detected using sequence bands, because of OH $A^2\Sigma$ predissociation. It is plausible that the amount of OH presently undetected (i.e. $v \geqslant 2$) is comparable with the combined $v = 0$ and 1 populations.

With N_2O–HI complexes, however, the amount of OH rotational excitation is dramatically reduced compared with bulk conditions as shown in figure 9. The $[v = 1]/[v = 0]$ ratio is *ca.* 0.4, neglecting $v = 0$ rotational states above the experimental limit under bulk conditions. We regard this significantly colder OH internal excitation under complexed conditions as a manifestation of its interaction with the nearby I atom. The effect of such interaction on translational degrees of freedom was previously observed as a significant lowering in translational energy of the OH product from N_2O–HBr PGL environments relative to bulk conditions (Chen *et al.* 1989). Thus, both OH rotational and translational excitations are much less due to the HO–X interaction under N_2O–HX complexed conditions than under bulk conditions, while NH shows no such striking change (Chen *et al.* 1990). Although the HN–X interaction is probably as attractive as the HO–X interaction, however, for the case of HN–NO fragmentation, the X–NO interaction is supposedly more attractive and geometrically more favourable than HN–X once the H atom has shifted to the terminal nitrogen. Also, the lifetime of the HNNO† intermediate may lead to a sufficiently large HNNO–X distance at the point of fragmentation that HN–X exit channel interactions are not present to any significant extent. In the same way, the CO_2–HBr system yielding OH products via long-lived HOCO† intermediates has shown to have slightly colder but similar OH translational distributions under complexed conditions compared with bulk conditions (Chen *et al.* 1989). Therefore, the $OH + N_2$ channel with no such long-lived intermediate is anticipated to experience more interactions with the nearby X atom than other channels involving long-lived intermediates.

Perhaps the most interesting observation is the change in the relative NH and OH populations between bulk and complexed conditions for the same photolysis wavelength. Note the rather small NH population in figure 10*b* compared with figure 10*a*. The (*a*) and (*b*) entries are normalized to one another by setting the OH($v = 0$) populations equal. The [NH]/[OH] ratio, for the observed OH levels, drops by a factor of 12 in going from bulk to complexed conditions. With the total OH population estimated by summing the geometric progression of 0.5 and 0.4 for bulk and complex conditions, respectively, up to the energetically allowed highest vibrational level, the bulk [NH]/[OH] ratio is a factor of 10 higher than with complexed conditions. However, k_{2b} depends sensitively on available energy, in contrast to k_{2a} (Chen *et al.* 1990). Consequently, an enhancement factor was estimated, assuming that the total available energy is reflected in the NH rotational distribution and ignoring exit channel interactions with the I atom. The NH rotational distribution deriving from 251 nm N_2O–HI photolysis corresponds to
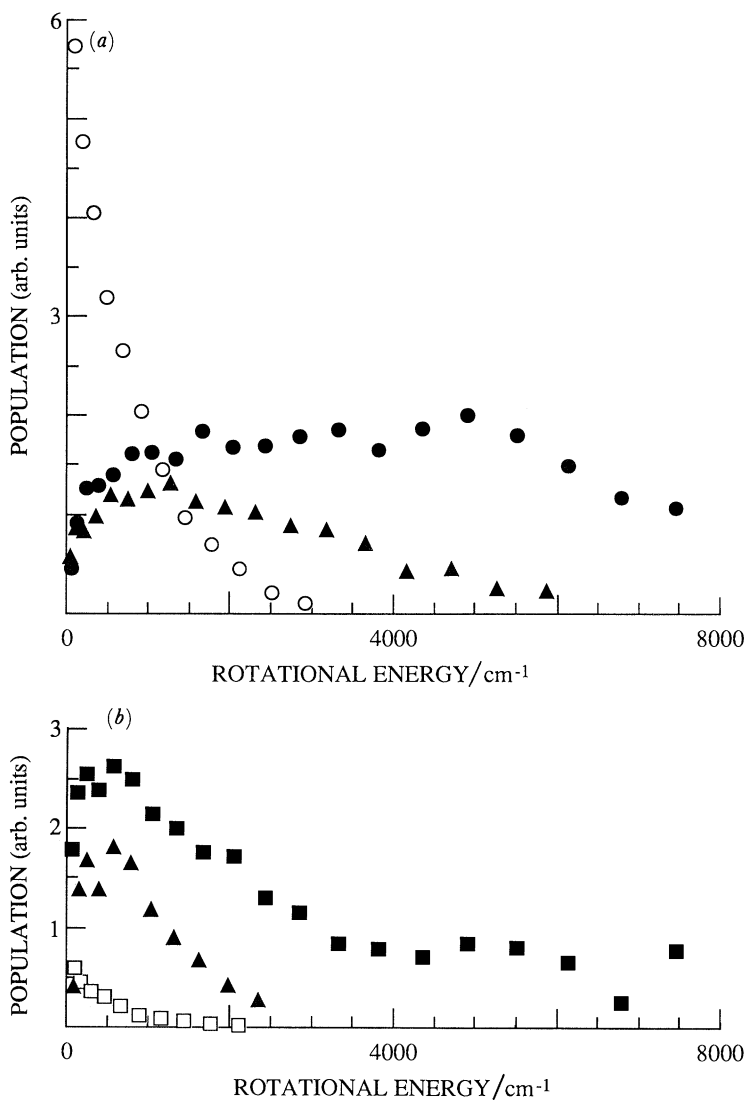
Figure 10. Branching ratio measurements showing relative NH and OH $v = 0$ and 1 rotational populations for (a) bulk and (b) complexed conditions, using 251 nm photolysis. ●, ■, OH ($v = 0$); ▲, OH ($v = 1$); ○, □, NH.

259 nm bulk photolysis, and we determined experimentally that (bulk) [NH]/[OH] is a factor of three lower at 259 nm than 251 nm (Chen *et al.* 1990). Thus, the observed factor of 10–12 cannot be assigned solely to a lowering of the energy. It may be due in part or whole to the large entrance channel stereospecificity of the PGL environment. Other possible explanations, such as termolecular interactions (e.g. yielding NHI + NO) and OH vibrational relaxation await further investigation.

The data shown in figure 10 show a marked effect, with the change of the [NH]/[OH] ratio in going from bulk to complexed conditions suggesting more favourable oxygen than nitrogen side attacks. This is a valuable result, showing that significant influences on chemically distinct product channels can be forthcoming when reactions are initiated in complexes. From our experience with $N_2O–HX$

(X = F, Cl, Br), where O–H bonding is proven or suspected (Zeng *et al.* 1990) it is tempting to infer that N_2O–HI localizes the H atoms that go on to react nearer the oxygen than nitrogen. This may well turn out to be the case, which then suggests a straightforward interpretation of the experimental results: entrance channel geometric specificity dictates the route travelled in forming products.

References

Anderson, W. R. 1989 *J. phys. Chem.* **93**, 530.

Beuhler, B. J., Bernstein, R. B. & Kramer, K. H. 1966 *J. Am. chem. Soc.* **88**, 5332.

Breckenridge, W. H., Jouvet, C. & Soep, B. 1986 *J. chem. Phys.* **85**, 1443.

Brooks, P. R. 1969 *J. chem. Phys.* **50**, 5031.

Brooks, P. R. 1976 *Science, Wash.* **193**, 11.

Burlow, S., Radhakrishnan, G., Catanzarite, J. & Wittig, C. 1985 *J. chem. Phys.* **83**, 444.

Buelow, S., Noble, M., Radhakrishnan, G., Reisler, H., Wittig, C. & Hancock, G. 1986 *J. phys. Chem.* **90**, 1015.

Buelow, S., Radhakrishnan, G. & Wittig, C. 1987 *J. phys. Chem.* **91**, 5409.

Chen, Y., Hoffmann, G., Oh, D. & Wittig, C. 1989*a* *Chem. Phys. Lett.* **159**, 426.

Chen, Y., Hoffmann, G. & Wittig, C. 1989*b* *J. chem. Soc. Faraday Trans.* II **85**, 1292.

Chen, Y., Hoffmann, G., Shin, S. K., Oh, D., Sharpe, S. W., Zeng, Y. P., Beaudet, R. A. & Wittig, C. 1990*a* In *Advances in molecular vibrations and collision dynamics* (ed. J. M. Bowman). JAI. (Submitted.)

Chen, Y., Shin, S. K., Hoffmann, G. & Wittig, C. 1990*b* (In preparation.)

Chidsey, I. L. & Crosley, D. R. 1980 *J. quant. Spectrosc. radiat. Transfer* **23**, 187.

Dimpfl, W. L. & Kinsey, J. L. 1979 *J. quant. Spectrosc. radiat. Transfer* **21**, 233.

Dixon, R. N. 1959 *Can. J. Phys.* **37**, 1171.

Dixon-Lewis, G. & Williams, D. J. 1977 In *Gas-phase combustion, comprehensive chemical kinetics* (ed. C. H. Bamford & C. F. H. Tipper), vol. 17. Amsterdam: Elsevier.

Duval, M. C., Benoist-D'Azy, O., Breckenridge, W. H., Jouvet, C. & Soep, B. 1986 *J. chem. Phys.* **85**, 6324.

van den Ende, D. & Stolte, S. 1980 *Chem. Phys. Lett.* **76**, 13.

Fairchild, P. W., Smith, G. R., Crosley, D. R. & Jeffries, J. B. 1984 *Chem. Phys. Lett.* **107**, 181.

Flynn, G. W. & Weston, R. E. 1986 *A. Rev. phys. Chem.* **37**, 551.

Gandhi, S. R., Curtiss, T. J., Xu, Q. X., Choi, S. E. & Bernstein, R. B. 1986 *Chem. Phys. Lett.* **132**, 6.

Gandhi, S. R., Xu, Q. X., Curtiss, T. J. & Bernstein, R. B. 1987 *J. phys. Chem.* **91**, 5437.

Hausler, D., Rice, J. & Wittig, C. 1987 *J. phys. Chem.* **91**, 5413.

Hoffmann, G., Oh, D., Lams, H. & Wittig, C. 1989*a* *Chem. Phys. Lett.* **155**, 356.

Hoffmann, G., Oh, D. & Wittig, C. 1989*b* *J. chem. Soc. Faraday Trans.* II **85**, 1141.

Hollingsworth, W. E., Subbiah, J., Flynn, G. W. & Weston Jr, R. F. 1985 *J. chem. Phys.* **82**, 2295.

Johnson, M. A., Allison, J. & Zare, R. N. 1986 *J. chem. Phys.* **85**, 5723.

Jouvet, C. & Soep, B. 1983 *Chem. Phys. Lett.* **96**, 426.

Jouvet, C., Duval, M. C. & Soep, B. 1987 *J. phys. Chem.* **91**, 5416.

Karny, Z., Estler, R. C. & Zare, R. N. 1978 *J. chem. Phys.* **69**, 5199.

Kleinermanns, K. & Wolfrum, J. 1983*a* *Laser Chem.* **2**, 339.

Kleinermanns, K. & Wolfrum, J. 1983*b* *Chem. Phys. Lett.* **104**, 157.

Kleinermanns, K., Linnebach, E. & Wolfrum, J. 1985 *J. phys. Chem.* **89**, 2525.

Kramer, K. H. & Bernstein, R. B. 1965 *J. chem. Phys.* **42**, 767.

Levine, R. D. & Bernstein, R. B. 1987 *Molecular reaction dynamics and chemical reactivity*. Oxford, New York.

Lowry, T. H. & Richardson, K. S. 1981 *Mechanism and theory in organic chemistry*, 2nd edn, pp. 120–122. New York: Harper and Row.

Marcellia, G. & Brooks, P. R. 1975 *J. Am. chem. Soc.* **97**, 1710.

Marshall, P., Fontijn, A. & Melius, C. F. 1987 *J. chem. Phys.* **86**, 5540.

Marshall, P., Ko, T. & Fontijn, A. 1989 *J. phys. Chem.* **93**, 1922.

Ohoyama, H., Takayanagi, M., Nishiya, T. & Hanazaki, I. 1989 *Chem. Phys. Lett.* **162**, 2.

Parker, D. H., Chakravorty, K. K. & Bernstein, R. B. 1981 *J. phys. Chem.* **85**, 466.

Parker, D. H., Jalink, H. & Stolte, S. 1987 *J. phys. Chem.* **91**, 5427.

Quick, C. R. & Tiee, J. J. 1983 *Chem. Phys. Lett.* **100**, 223.

Radhakrishnan, G., Buelow, S. & Wittig, C. 1986 *J. chem. Phys.* **84**, 727.

Rettner, C. T. & Zare, R. N. 1982 *J. chem. Phys.* **77**, 2416.

Rice, J., Hoffmann, C. & Wittig, C. 1988 *J. chem. Phys.* **88**, 2841.

Schatz, G. C. & Fitzcharles, M. S. 1988 In *Selectivity in chemical reactions* (ed. J. C. Whitehead). Dordrecht: Klumer.

Schatz, G. C., Fitzcharles, M. S. & Harding, L. B. 1987 *Faraday Discuss. chem. Soc.*

Scherer, N. F., Khundkar, L. R., Bernstein, R. B. & Zewail, A. H. 1987 *J. chem. Phys.* **87**, 1451.

Scherer, N. F., Sipes, C., Bernstein, R. B. & Zewail, A. H. 1990 *J. chem. Phys.* (Submitted.)

Sharpe, S. W., Zeng, Y. P., Wittig, C. & Beaudet, R. A. 1990 *J. chem. Phys.* **92**.

Smith, I. W. M. 1980 *Kinetics and dynamics of elementary gas reactions*. Toronto: Butterworths.

Stolte, S. 1982 *Ber. BunsenGes. phys. Chem.* **86**, 413.

Stolte, S. 1987 In *Atomic and molecular beam methods* (ed. G. Scoles), vol. 1, ch. 25. Oxford, New York.

van Veen, G. N. A., Mohamed, K. A., Baller, T. & de Vries, A. E. 1983 *Chem. Phys.* **80**, 113.

Wittig, C., Engel, Y. M. & Levine, R. D. 1988*a* *Chem. Phys. Lett.* **153**, 411.

Wittig, C., Sharpe, S. & Beaudet, R. A. 1988*b* *Acct. chem. Res.* **21**, 341.

Zare, R. N. 1982 *Ber. BunsenGes. phys. Chem.* **86**, 422.

Zehnacker, A., Duval, M. C., Jouvet, C., Lardeux-Dedonder, C., Solgadi, D., Soep, B. & Benoist D'Azy, O. 1987 *J. chem. Phys.* **86**, 6565.

Zeng, Y. P., Sharpe, S. W., Reifenschneider, D., Wittig, C. & Beaudet, R. A. 1990 *J. chem. Phys.* (In the press.)

Zewail, A. H. 1988 *Science, Wash.* **242**, 1645.

Zewail, A. H. & Bernstein, R. B. 1988 *Chem. Engng News* **66**, 24.